Separation and Purification Technology 330 (2024) 125329

Contents lists available at ScienceDirect

Separation and Purification Technology

journal homepage: www.elsevier.com/locate/seppur

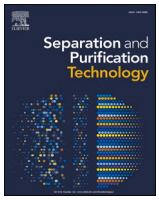

Highly permeable ZIF-8 membranes for C_2H_4/C_2H_6 separation in a wide temperature range

Marta Pérez Miana [a,b], Joaquín Coronas [a,b], Jonas Hedlund [c], Liang Yu [c,*]

[a] Instituto de Nanociencia y Materiales de Aragón (INMA), CSIC-Universidad de Zaragoza, 50018 Zaragoza, Spain
[b] Chemical and Environmental Engineering Department, Universidad de Zaragoza, 50018 Zaragoza, Spain
[c] Chemical Technology, Luleå University of Technology, SE-971 87 Luleå, Sweden

ARTICLE INFO

Editor: Gaohong He

Keywords:
Ultrathin ZIF-8 membranes
High permeability
Olefin/paraffin separation
Ethylene
Ethane

ABSTRACT

Ethylene/ethane separation is a critical and energy-consuming process in the chemical industry due to the similar properties of the compounds and the great need of ethylene for e.g., polymer production. Many materials have been studied for their implementation as membranes as an energetically favorable alternative to conventional distillation and adsorption processes. Metal-organic frameworks (MOF) have revealed promising properties as highly permeable and selective membranes. Among the most studied and promising MOF candidates is ZIF-8, known for its thermal stability and small pores connected by narrow-sized windows. In this work, we present an analysis of the influence of parameters such as temperature, feed pressure and feed flowrate on the separation of ethylene/ethane through a thin ZIF-8/alumina disc membrane. We observed that the temperature has a significant effect on the separation. The ethylene permeance increased with decreased temperature and reached 8.1 $\times$ 10^{-7} mol/(m^2·s·Pa) at −30 °C. At this temperature, the ethylene/ethane selectivity was 2.5. The study concluded with a considerable enhancement of the permeance of ZIF-8 membranes for ethylene/ethane separations, while maintaining a good selectivity compared to the reported values in the literature. The results have important implications for the development of more cost-effective and energy-efficient membrane-based separation technologies for ethylene purification.

1. Introduction

Ethylene (C_2H_4), as an important feedstock in the industry, is commonly produced through steam cracking using ethane (C_2H_6) or naphtha as feedstock. A mixture of C_2H_4/C_2H_6 is obtained from the process due to the chemical equilibrium. One of the main uses of C_2H_4 is in polymer production, where a high purity (99.9 wt%) is necessary. However, the separation of C_2H_4/C_2H_6 is challenging because of the similar properties of the molecules, shown in Table 1.

For industrial separation by conventional cryogenic distillation, a low-temperature splitter with up to 200 trays in the column is needed [1], and the feed to the distillation splitter consists of an ethylene-ethane saturated vapor mixture at about − 24 °C and 21 bar. To facilitate cryogenic distillation in the column using a readily available propylene refrigerant at −36 °C as coolant, a high column pressure of around 19 bar is needed [2]. The high pressure and low temperature process demands a huge amount of energy and thereby high costs. Therefore, the development of new energy-efficient separation technologies is of great interest. Given this scenario, membrane technology has emerged as an energetically favorable alternative with a much lower energy demand compared with distillation processes [3,4]. Also, hybrid membrane-distillation and membrane-adsorption processes are viable alternatives as an initial implementation [5]. In any case, high quality membranes are needed.

Polymeric membranes are used in industrial gas separation processes. However, for olefin/paraffin separations, the mass transfer occurs through a sorption–diffusion mechanism, which results in low selectivity for molecules with similar adsorption coefficients. This is the case for separation of C_2H_4/C_2H_6 [6,7]. Copolyimides are promising polymers as dense membranes for C_2 hydrocarbon separations [8–11]. The highest C_2H_4/C_2H_6 selectivity of 6.8 is reported for 4,4′-(hexafluoroisopropylidene) diphthalic anhydride-1,5-naphthalene diamine (6FDA-NDA) copolyimides [8], however, the C_2H_4 permeability is only 1.2 Barrer (8×10^{-12} mol/(m^2·s·Pa) for a membrane thickness of 50 μm) [9]. A polymer of intrinsic microporosity membrane (PIM-1, 2,3,5,6-tetrafluorophthalonitrile-3,3,3′,3′-tetramethyl-1,1′-spirobisin dane-

* Corresponding author.
E-mail address: liang.yu@ltu.se (L. Yu).

https://doi.org/10.1016/j.seppur.2023.125329
Received 21 July 2023; Received in revised form 29 September 2023; Accepted 8 October 2023
Available online 10 October 2023

Table 1
Some crucial properties for ethylene/ethane separations.

Components	Kinetic diameter (nm)	Polarizability × 10^{25} (cm)	Critical temperature (K)	Boiling point (K)
Ethylene	0.423	42.5	282	169
Ethane	0.442	44.5	305	184

5,5′,6,6′-tetrol *co*-polymer) [12] displayed a higher C_2H_4 permeability of 535 Barrer (3.6×10^{-9} mol/(m^2·s·Pa) at a membrane thickness of 50 μm) at a feed pressure of 1 bar, but a low C_2H_4/C_2H_6 selectivity of 1.4. The selectivity was lost when the feed pressure was increased to 10 bar. PIM-6FDA and PIM-6FDAOH membranes were investigated by Salinas et al. [13,14], and their hydroxyl groups enhanced the selectivity with slightly compromised C_2H_4 permeability, but they did not exceed the C_2H_4/C_2H_6 polymer upper bound (although the membrane overcame the C_3H_6/C_3H_8 polymer upper bound [8]). In addition, plasticization is also an important issue for polymeric membranes, which could reduce the separation performance of the polymeric membrane significantly [12].

Other membrane types, e.g., carbon molecular sieve membranes (CMS) [14–16], mixed-matrix membranes (MMMs) [17], zeolite membranes [18], and MOF membranes could offer improved stability as well as selectivity by taking advantage of entropic diffusion selectivity. Carbon membranes have exceeded the upper limit of polymeric membranes for C_2H_4/C_2H_6 separation. The transport properties of CMS are dependent on a pore structure resembling narrow slits, characterized by a network of larger micropores (approximately 7–20 Å in size) interconnected by smaller ultramicropore windows (less than 7 Å in size) [15]. M-gallate ($M(C_7O_5H_4)\cdot H_2O$, M = Ni, Co, Mg) MOFs-based mixed matrix membranes showed greater performance for C_2H_4/C_2H_6 separation compared to the pure polymeric membranes [19]. UTSA-280 with superb C_2H_4/C_2H_6 adsorption selectivity also enhanced the C_2H_4 permeability and C_2H_4/C_2H_6 separation selectivity of polyimides membranes by 15% and 32%, respectively [20].

Zeolite [18] and MOF membranes have been studied due to their greater potential to overcome thermal, chemical, and mechanical stability issues as well as to achieve higher separation performance [21,22]. In 2001, Nikolakis et al. reported the first use of microporous FAU-type zeolite NaX membranes for olefin/paraffin separation [23]. Later, Sakai et al. [24] reported an C_2H_4/C_2H_6 selectivity of 16 with an C_2H_4 permeance of 9×10^{-8} mol/(m^2·s·Pa) for a zeolite AgX membrane containing silver ions. MOF is also an example of crystalline microporous materials that have been implemented as membranes for olefin/paraffin separations revealing much higher separation performance than most porous materials [25]. Among them, ZIFs (zeolitic imidazolate framework), one type of MOFs with imidazolate ligands, have been studied intensively as membrane material for olefin/paraffin separation because of their high porosity [26], flexible pore architecture and functionality [27,28], and high thermal stability (up to 400 °C) [29]. ZIF-8 (a Zn 2-methylimidazolate (mIm), i.e. $Zn(mIm)_2$) crystals present a SOD-type structure with large cages (11.6 Å in diameter) connected through small apertures (0.34 nm) [30]. ZIF-8 membranes showed good separation selectivity and permeance for separation of C_2H_4/C_2H_6 mixtures. Bux et al. [31] observed an C_2H_4/C_2H_6 separation selectivity of 2.8 and an C_2H_4 permeance of 1.8×10^{-8} mol/(m^2·s·Pa) at a feed pressure of 1 bar and a temperature of 25 °C, and the selectivity decreased to 2.4 when the feed pressure increased to 6 bar. An ideal selectivity of 4.2 was observed at a feed pressure of 6 bar. James et al. [32] also reported an C_2H_4/C_2H_6 mixture selectivity of around 2.0 and an C_2H_4 permeance of 7.8×10^{-8} mol/(m^2·s·Pa) for ZIF-8 membranes at a feed pressure of 1 bar. An ideal selectivity of 2.3 was observed at a membrane temperature of 25 °C. The effect of temperature was also studied, and it was observed that the permeance decreased with increasing temperature from 25 to 100 °C, and that the membrane was slightly less selective with a separation selectivity of 2.1 at 100 °C. No data was reported for membrane temperatures lower than 25 °C. Recently, the Co-gallate MOF membranes reported by Sun et al showed a high C_2H_4/C_2H_6 mixture separation factor of about 8, the corresponding C_2H_4 permeance was 2.5×10^{-8} mol/(m^2·s·Pa). The separation factor decreased from 8 to 6 when the temperature was increased from 20 to 100 °C, meanwhile, the C_2H_4 permeance was constant [33]. Oriented ZIF-8 membranes prepared on carbon nanotube support showed a high C_2H_4/C_2H_6 selectivity of about 9, which was 3 times higher than that of the randomly oriented ZIF-8 membranes and the C_2H_4 permeance of the oriented ZIF-8 membranes was about 8×10^{-8} mol/(m^2·s·Pa) [34].

Furthermore, it has been reported that the heat of adsorption of C_2H_6 (−17.1 kJ/mol) on ZIF-8 is more negative than that of C_2H_4 (−16.2 kJ/mol) [35]. However, it has been concluded [32] that the selectivity of the ZIF-8 membrane to C_2H_4 resulted from the narrow pore opening of ZIF-8 (0.34 nm [30]) and flexible structure. These factors favour the transport of the smaller molecule (C_2H_4 with a kinetic diameter of 0.41 nm as compared to C_2H_6 with a kinetic diameter of 0.44 nm) from a C_2H_4/C_2H_6 mixture. Other studies have also suggested that the effective aperture size of ZIF-8 for molecular sieving is between 0.40 and 0.42 nm by estimating the thermodynamically corrected diffusivities of probe molecules with different kinetic diameters [36]. The value is much larger than the pore size of 0.34 nm determined from XRD data. In the latter case, the effective pore size of ZIF-8 is slightly larger than the kinetic diameter of C_2H_4 and smaller than that of C_2H_6, which presumably would result in faster diffusion of the C_2H_4 molecule. The faster diffusion overcompensates the adsorption preference of C_2H_6, therefore, the ZIF-8 membrane is C_2H_4 selective [26]. However, owing to large thickness (>5 μm) of the studied membranes, the reported ZIF-8 membranes displayed quite low C_2H_4 permeance ($<2 \times 10^{-7}$ mol/(m^2·s·Pa)). Therefore, for a given separation task, a large membrane area is needed, which generates high cost. Since ZIF-8 membranes are more expensive than polymeric membranes, membranes with high permeability are necessary in order to be competitive.

In the present study, ultra-thin ZIF-8 membranes were synthesized and evaluated for the separation of C_2H_4/C_2H_6. The membrane was characterized using SEM and XRD and by single component permeation experiments for gases with different kinetic diameters. In addition, single component permeation experiments of C_2H_4 and C_2H_6 were performed in a wide temperature range. Finally, permeation experiments for an equimolar C_2H_4/C_2H_6 feed mixture were performed at different feed flowrates, pressures, and temperatures. So far, MOF membrane separation at relatively high temperatures has been studied extensively and the study on low-temperature separation is scarce. In addition, the gas temperatures could be high or low after the removal of water and some other impurities, which depends on the techniques used in the industry. Therefore, membrane separation at low temperatures is necessary for some cases. Considering the feed temperature in conventional cryogenic distillation processes could be as low as −24 °C [2] in the industry, the membrane separation experiments were performed in a wide temperature range of −30 to 100 °C in the present work.

2. Experimental

2.1. Materials synthesis and characterization by SEM and XRD

ZIF-8 membranes used in this study were developed by ZeoMem Sweden AB. The membranes were synthesized by seeding and growth. A seed suspension of ZIF-8 nanocrystals (ca. 80 nm) in methanol was prepared as described in a previous work [37]. Briefly, a zinc nitrate aqueous solution was prepared by dissolving 1.0 g of zinc nitrate hexahydrate (98% Sigma-Aldrich) in 4 g deionized water. This solution was added to a 2-methylimidazole (99% Sigma-Aldrich) aqueous solution under vigorous stirring condition at room temperature. The 2-methylimidazole aqueous solution was prepared by dissolving 11.4 g of 2-methylimidazole in 40 g deionized water. ZIF-8 nanocrystals were

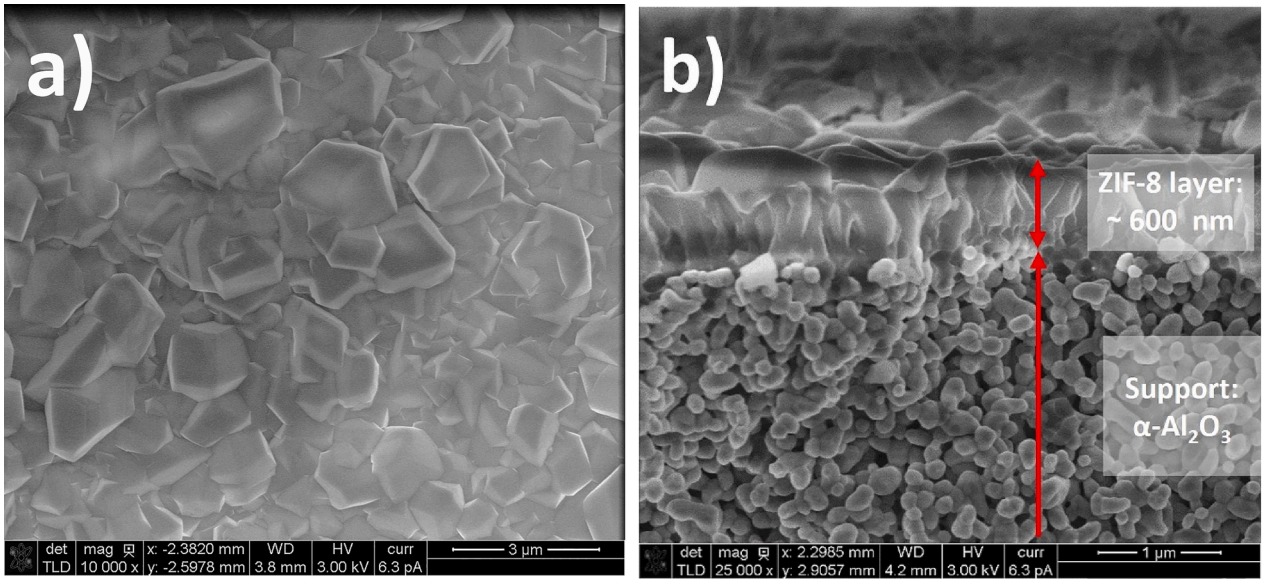

Fig. 1. A) top-view and b) cross-sectional sem images of a zif-8 membrane.

recovered using centrifuge, and then redispersed in methanol (1 wt% ZIF-8 nanocrystals in methanol).

The membranes were supported on porous α-alumina discs with a pore size of about 100 nm. The thickness of the disc is 3 mm, and the diameter is 25 mm. Prior to seeding, the support was calcined at 500 °C for 6 h and cooled down to room temperature naturally. The support was then rinsed by deionized water and immersed in a cationic polymeric solution (1 wt% commercial cationic polymer (Redifloc 4150, Eka Chemicals AB, Sweden) in water) for 15 min. Afterwards, the supports were rinsed by water to remove excess polymer from the surface of the supports. The rinsed supports were immersed in the ZIF-8 suspension for 15 min and then rinsed by methanol to obtain seeded supports. Subsequently, the seeded supports were immersed in a ZIF-8 membrane synthesis mixture and maintained at 30 °C for 2 h. The mass ratio of the membrane synthesis mixture was 1 g zinc nitrate hexahydrate/21 g 2-methylimidazole/365 g water. The as-synthesized ZIF-8 membranes were rinsed thoroughly by methanol and dried at room temperature.

A scanning electron microscope (SEM, FEI Magellan 400 field emission) was employed to investigate the morphology of the membranes at an accelerating voltage of 3 kV and an emission current of 3 pA. Due to the low landing energy and the purpose of preserving the original morphology, no conductive coating was used on the membranes for SEM analysis. A PANalytical Empyrean diffractometer equipped with a Cu Kα1 ($\lambda = 0.1541$ nm) LFF HR X-ray tube and a PIXcel^{3D} detector was used to record the X-ray diffraction (XRD) patterns from 5 to 30°with a scanning rate of 0.03°/s. The voltage and current of the generator were 45 kV and 40 mA, respectively. HighScore software combined with the ICDD (the International Centre for Diffraction Data) database was used to analyze the recorded XRD patterns.

2.2. Single component and binary mixture permeation experiments

The membrane was sealed in a stainless steel Wicke–Kallenbach cell using graphite gaskets for all permeation experiments. The inner diameter of the gasket was 18 mm. Single component permeation experiments of He, H_2, CO_2, N_2, CH_4, C_2H_4, C_2H_6 and SF_6 were carried out at room temperature using a feed pressure of 1.5 bar and atmospheric permeate pressure. No sweep gas was used and the flow rate on the permeate side was monitored by a bubble flowmeter.

Single component permeation experiments using C_2H_4 and C_2H_6 were also carried out in a temperature range of −30 to 100 °C at feed and permeate pressures of 1 bar. A flow rate of about 150 NmL/min of helium was used as sweep gas. Single component permeation experiments using C_2H_4 and C_2H_6 were also performed at feed pressures from 1 to 4 bar at a constant membrane temperature of −30 °C. The permeate pressure was 1 bar and helium was used as sweep gas (150 NmL/min). The flow rate on the permeate side was measured using a bubble flowmeter. An online Micro GC (Agilent 490) was used to analyze the composition of the permeate. For experiments at sub-ambient membrane temperatures, the cell was placed in a container, which was cooled with recirculating silicone oil provided by a cooling bath.

Permeation experiments for an equimolar C_2H_4/C_2H_6 mixture were performed in continuous flow mode. To optimize the feed flow rate, the experiment was first carried out at different feed flowrates in the range of 300–1600 NmL/min using a Brooks mass flow controller. A back pressure regulator on the retentate line was used to control the feed pressure, and digital pressure gauges were used to monitor the pressure at both sides of the membrane. Then, the experiments were performed in a temperature range of −30 to 100 °C, and feed pressure range of 1–4 bar using the optimum feed flowrate. The permeate pressure was 1 bar and helium was used as sweep gas at a flow rate of about 150 NmL/min. The flow rate of sweep gas would affect the partial pressures of C_2H_4 and C_2H_6 on the permeate side of the membrane. Therefore, the separation results may be different. However, in this study, the flow rate of sweep gas was maintained constant in all permeation experiments. A bubble flow meter was used to monitor the flowrate on the permeate side and an online Micro GC (Agilent 490) was used to analyze the composition.

The permeance of C_2H_4 was calculated using Equation (1):

$$\Pi_{C_2H_4} = \frac{F_{C_2H_4}}{A\Delta P_{C_2H_4}} (\mathrm{mol}/(\mathrm{m}^2 \bullet \mathrm{s} \bullet \mathrm{Pa})) \quad (1)$$

In *Equation (1)*, $F_{C_2H_4}$ is the molar flow rate (mol/s) of C_2H_4 on the permeate side, which was calculated based on the volumetric flow rate and composition of the gas stream on the permeate side. A (m^2) is the actual membrane area for separation and $\Delta P_{C_2H_4}$ (Pa) is the partial pressure difference of C_2H_4 on the feed and permeate side of the membrane. The same formula was used to calculate the permeance of C_2H_6 (Equation (2)):

$$\Pi_{C_2H_6} = \frac{F_{C_2H_6}}{A\Delta P_{C_2H_6}} (\mathrm{mol}/(\mathrm{m}^2 \bullet \mathrm{s} \bullet \mathrm{Pa})) \quad (2)$$

The selectivity $\alpha_{C_2H_4/C_2H_6}$ of the membrane for C_2H_4 over C_2H_6 was calculated using Equation (3):

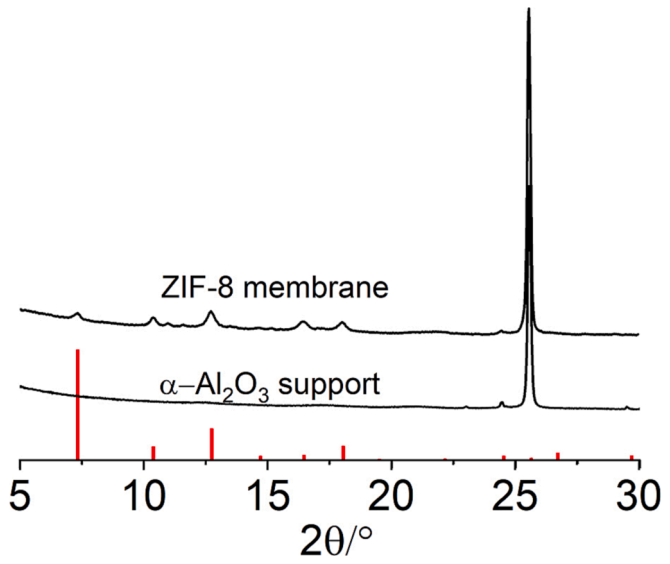

Fig. 2. XRD pattern of a ZIF-8 membrane and α-Al_2O_3 support. The red bars represent the reference pattern of ZIF-8 (ICDD PDF card number: 00-062-1030). (For interpretation of the references to colour in this figure legend, the reader is referred to the web version of this article.)

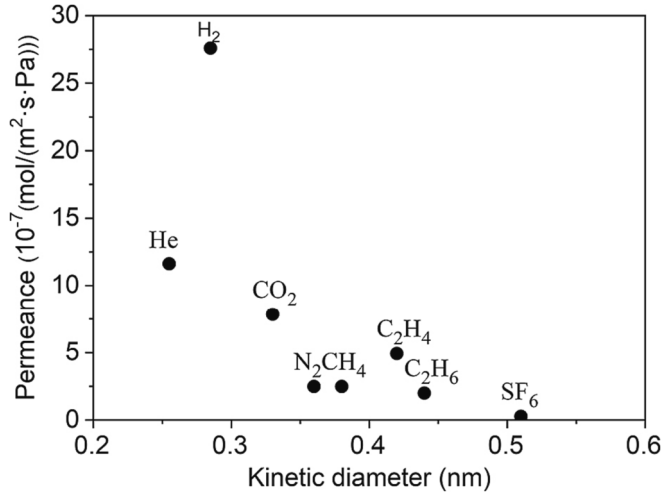

Fig. 3. Single component permeances at room temperature as a function of the kinetic diameter of the respective molecule.

$$\alpha_{C_2H_4/C_2H_6} = \frac{\Pi_{C_2H_4}}{\Pi_{C_2H_6}} \quad (3)$$

3. Results and discussion

3.1. Characterization by SEM and XRD

A top-view SEM image (Fig. 1a) of the ZIF-8 membrane shows that the film is continuous and composed of well-intergrown crystals with a rombododecahedral habit, characteristic of the ZIF-8 phase. The surface appears clean, and no defects in the film could be observed by SEM. The cross-sectional SEM image (Fig. 1b) reveals a uniform and continuous ZIF-8 film layer with a thickness of around 600 nm. This thickness is much lower than for other ZIF-8 membranes reported in the literature as discussed in the introduction section. The porous support is clean, and no invasion of MOF material is observed by SEM in the pores of the support. This is important since such invasion would increase the mass transport resistance [38].

Fig. 2 presents the XRD patterns of the ZIF-8 membrane and α-Al_2O_3 support. The XRD patterns show typical reflections from the ZIF-8 and α-Al_2O_3 phases, no other phase was detected as concluded by comparison with the reference pattern of ZIF-8 (ICDD PDF card number: 00-062-1030). The reflections from the ZIF-8 phase were relatively weak as a result from the ultra-thin ZIF-8 film.

3.2. Single component permeation

The measured single component permeances at room temperature are presented in Fig. 3. The observed He single component permeance was 12 × 10^{-7} mol/(m^2·s·Pa), i.e. 4 times higher than the permeance reported by James et al. for a 5 μm film (3.1 × 10^{-7} mol/(m^2·s·Pa)) [32]. The membrane also displayed a high H_2 permeance of 28 × 10^{-7} mol/(m^2·s·Pa) that was 10 times higher than the reported H_2 permeance of 2.8 × 10^{-7} mol/(m^2·s·Pa) [32]. The very high He and H_2 permeances observed in the present work are a result of the very thin film with a thickness of just 600 nm in combination with no invasion in the support as observed by SEM. On the contrary, a very low SF_6 permeance of 2.6 × 10^{-8} mol/(m^2·s·Pa) was observed in the present work. Since the kinetic diameter of SF_6 (0.51 nm) is much larger than the pore size of ZIF-8, the low SF_6 permeance indicates a membrane with low density of defects. The value of SF_6 permeance may be considered not as low as the values for ZIF-8 membranes reported in the literature. However, if we consider He and SF_6 permeances (12 × 10^{-7} and 2.6 × 10^{-8} mol/(m^2·s· Pa)) and its corresponding He/SF_6 ideal selectivity of 44, this value is notably higher than the Knudsen selectivity of 6, which suggests that it is a high-quality thin film layer of ZIF-8. If we also contemplate the H_2 permeance (28 × 10^{-7} mol/(m^2·s·Pa)) and the H_2/SF_6 ideal selectivity, this value increase one order of magnitude to a value of 106.

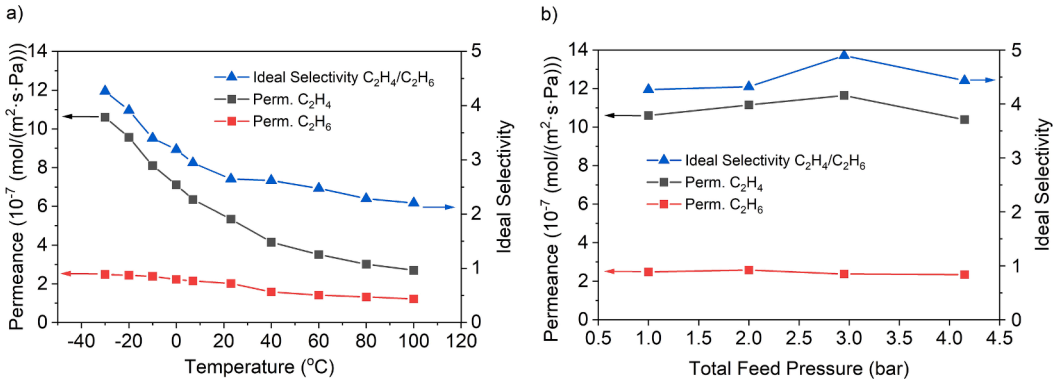

Fig. 4. C_2H_4 and C_2H_6 single component permeances (left axis) and ideal selectivity C_2H_4/C_2H_6 (right axis) as a function of temperature at a feed pressure of 1 bar (a) and as a function of feed pressure at −30 °C (b).

The single component permeances of C_2H_4 and C_2H_6 were 5.0 and 2.0 × 10^{-7} mol/(m^2·s·Pa), respectively, and the corresponding C_2H_4/C_2H_6 ideal selectivity was 2.5. These C_2H_4 and C_2H_6 permeances were much higher than the respective reported permeances of 0.78 × 10^{-7} mol/(m^2·s·Pa) and 0.39 × 10^{-7} mol/(m^2·s·Pa), respectively, by James et al. [32] or 0.2 × 10^{-7} mol/(m^2·s·Pa) and 0.1 × 10^{-7} mol/(m^2·s·Pa) reported by Bux et al. [31]. At the same time, the ideal selectivity of 2.5 observed in the present work was slightly higher than the ideal selectivity of 2.0 observed by James et al. and Bux et al. [31,32]. All the results observed here show that the membrane in the present work was highly permeable and had few defects, in agreement with the thin ZIF-8 film layer, open support, and well intergrown ZIF-8 crystals.

The single gas permeance of C_2H_4 observed in the present work was higher than the single gas permeance of N_2 and CH_4, even though the molecular size of the first is larger. This must be a result of the higher heat of adsorption of C_2H_4 (−16.2 kJ/mol) on ZIF-8 as compared to the heats of adsorption of N_2 (−13.4 kJ/mol) [39] and CH_4 (-11.8 kJ/mol) [40]. The higher heat of adsorption of C_2H_4 is caused by the higher polarizability and quadrupole moment of C_2H_4 with values of 42.5 × 10^{25} cm^3 and 1.5 × 10^{26} esu cm^2, respectively, which are much higher than those of N_2 (17.4 × 10^{25} cm^3 and 1.5 × 10^{26} esu cm^2) and CH_4 (25.9 × 10^{25} cm^3 and 0 esu cm^2) [41,42].

The influence of the temperature on the single component permeances of C_2H_4 and C_2H_6 was studied at a feed pressure of 1 bar with 1 bar helium as sweep gas and the results are shown in Fig. 4a. The permeances of C_2H_4 and C_2H_6 increased with decreasing temperature, presumably due to more adsorption at lower temperatures. This should result in a higher difference in concentration of adsorbed molecules at the feed and permeate side of the membrane, i.e., increased driving force and thereby a higher permeance.

The C_2H_4 permeance increased from 2.7 × 10^{-7} to 11 × 10^{-7} mol/(m^2·s·Pa), i.e., by about 300% when the temperature was decreased from 100 to −30 °C. However, the C_2H_6 permeance only increased by 127%, from 1.1 × 10^{-7} to 2.5 × 10^{-7} mol/(m^2·s·Pa) although the heat of adsorption for this molecule is more negative than that for C_2H_4. This is due to the fact that the C_2H_6 molecules are larger than those of C_2H_4 and close to the effective pore windows of ZIF-8. As we reported in previous work, the surface barrier of molecules is dependent on the size of the molecules and the pore size [43]. Furthermore, the surface barrier may probably be caused by the "pore blocking" or "pore narrowing" of the microporous materials during the molecule uptake process [44]. The former causes the total blockage of most of the surface with only a tiny fraction left open. The latter would result in higher activation energy than the diffusion-limited uptake. Both cases cause an extreme reduction of the flux rate all over the external surface, thereby low flux. Consequently, the surface barrier for the larger C_2H_6 molecules in ZIF-8 pores is higher due to the high activation energy, and as a result, the permeance of C_2H_6 was lower than that of C_2H_4. Moreover, the permeances of both C_2H_4 and C_2H_6 increased with decreasing temperature because of more adsorption at lower temperatures. However, the permeance of C_2H_4 increased more significantly than that of C_2H_6, which was ascribed to the lower surface barrier and faster diffusion for the smaller C_2H_4 compared to that for C_2H_6 (in line with the kinetic diameters given in Table 1). Therefore, the synergetic effects of adsorption, surface barrier, and diffusion contributed to the higher C_2H_4 permeance and higher C_2H_4/C_2H_6 selectivity at lower temperatures. Furthermore, the differences in the surface barrier and diffusion for C_2H_4 and C_2H_6 resulted from their molecular size and pore size of ZIF-8 as discussed above. As a result, the ideal selectivity of C_2H_4/C_2H_6 continuously increased from 2.2 to 4.3 when the temperature decreased from 100 to −30 °C. Fig. 4b shows the influence of feed pressure on the single component permeance of C_2H_4 and C_2H_6 at −30 °C. The permeances of both C_2H_4 and C_2H_6 as well as the ideal selectivity were almost constant when the feed pressure increased from 1 to 4 bar. The first is due to the fact that the permeation flux increase is compensated by the augmentation of the pressure gradient; the second can be explained by the absence of defects in the membrane (in line with the low SF_6 permeance and with the high separation selectivity observed) through which pressure dependent viscous flow would be produced.

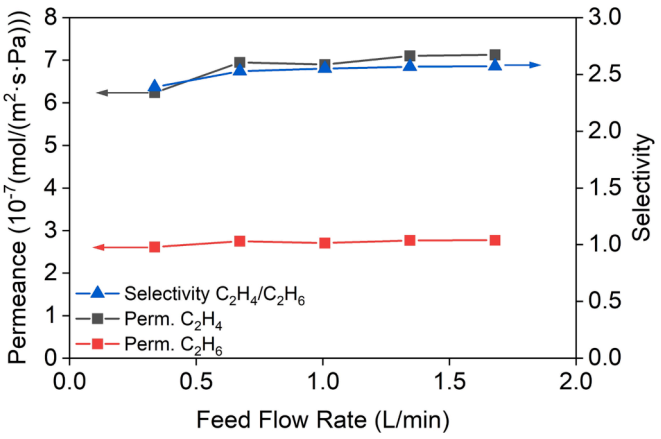

Fig. 5. Effect of feed flow rate on the C_2H_4 and C_2H_6 permeances (left-axis) and C_2H_4/C_2H_6 mixture selectivity (right-axis) for a feed comprising an equimolar C_2H_4/C_2H_6 mixture at a feed pressure of 1 bar and a membrane temperature of −30 °C.

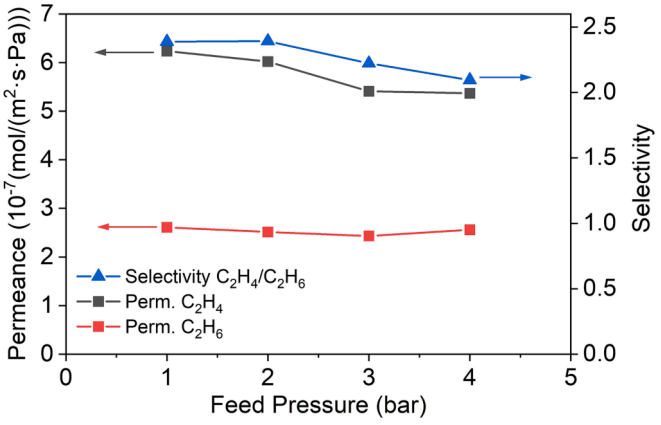

Fig. 6. Effect of feed pressure on the C_2H_4 and C_2H_6 permeances (left axis) and C_2H_4/C_2H_6 mixture selectivity (right axis) at a membrane temperature of −30 °C.

3.3. Separation of an ethylene/ethane (50/50) mixture

Since the highest permeance and ideal selectivity values were observed at −30 °C in the single gas experiment, the separation of the equimolar mixture was carried out at this temperature first. Fig. 5 illustrates the permeance and selectivity while varying the feed flow rate of an equimolar C_2H_4/C_2H_6 mixture at a membrane temperature of −30 °C. The feed pressure was 1 bar, and helium was employed as sweep gas. The C_2H_4/C_2H_6 mixture selectivity increased slightly from 2.4 to 2.6 when the feed flowrate increased from 340 to 1000 NmL/min. This can be ascribed to the effect of concentration polarization. The C_2H_4 permeance and C_2H_4/C_2H_6 mixture selectivity were almost constant when the feed flowrate was higher than 1000 NmL/min. To eliminate the effect of concentration polarization, a feed flow rate of 1000 mL/min was used for the following experiments.

To investigate the effect of feed pressure, an equimolar C_2H_4/C_2H_6 mixture was fed to the membrane while varying the feed pressure in the range from 1 to 4 bar. The membrane temperature was maintained at −30 °C, and the feed flow rate was kept constant at 1000 NmL/min and helium was employed as sweep gas. Fig. 6 illustrates the C_2H_4 and C_2H_6

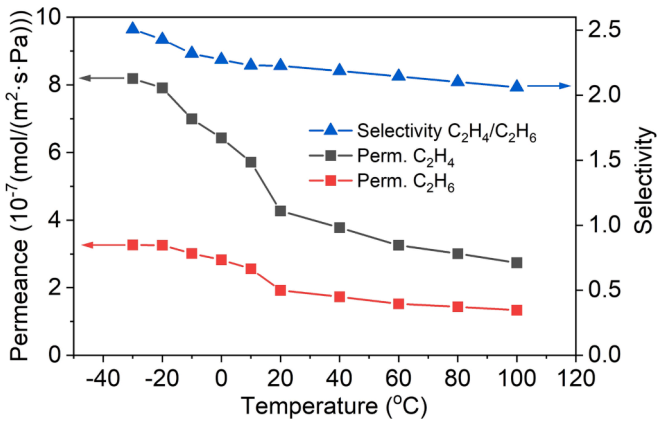

Fig. 7. Effect of temperature on the C_2H_4 and C_2H_6 permeances and C_2H_4/C_2H_6 separation selectivity for an equimolar C_2H_4/C_2H_6 mixture at a feed pressure of 1 bar.

permeances and C_2H_4/C_2H_6 mixture selectivity. The highest C_2H_4/C_2H_6 mixture selectivity was about 2.4 at a feed pressure of 1 bar, and it decreased to 2.1 at a feed pressure of 4 bar. The results show the optimum feed pressure was the atmospheric. This reduced selectivity at higher feed pressure may be associated to competitive adsorption of C_2H_6 in ZIF-8 at higher pressure [27].

Fig. 7 depicts permeances and C_2H_4/C_2H_6 mixture selectivity as a function of membrane temperature in the range of −30 to 100 °C at a feed pressure of 1 bar for an equimolar C_2H_4/C_2H_6 mixture. The highest C_2H_4 permeance was observed at the lowest investigated temperature (−30 °C) and was 8.1×10^{-7} mol/(m^2·s·Pa). The C_2H_4/C_2H_6 separation selectivity was 2.5 at −30 °C, lower than the ideal C_2H_4/C_2H_6 separation selectivity of 4.3 at the same temperature (see Fig. 4a), presumably due to the competitive adsorption of C_2H_6 in the mixture [32]. The C_2H_4/C_2H_6 mixture selectivity slightly decreased from 2.5 to 2.1 when the temperature increased from −30 to 100 °C. The observed separation selectivity follows the same trend as the ideal selectivity but is lower because of the explanation given above.

Table 2 summarizes the C_2H_4 permeances and C_2H_4/C_2H_6 mixture selectivities measured in this study and those reported in the literature for selected ZIF-8, polymer, and zeolite membranes. The observed permeance of the ZIF-8 membrane in the present work is significantly greater than those reported for polymeric and zeolite membranes. In addition, we observe a much higher C_2H_4 permeance than the reported values in the literature for ZIF-8 membranes. For instance, the C_2H_4 permeance reported by James et al. [32] was 10 times lower than the value we observed, which was most probably because their membrane was 10 times thicker than the membrane presented in this study. However, the C_2H_4/C_2H_6 separation selectivity reported by James et al. [32] was similar to ours. The C_2H_4 permeance reported by Valadez Sánchez et al. was quite high about 7×10^{-7} mol/(m^2·s·Pa). However, the C_2H_4/C_2H_6 mixture selectivity was only 1.3 at 1 bar and room temperature [46]. In the present work, the higher C_2H_4/C_2H_6 separation performance was mainly ascribed to the relatively higher C_2H_4 permeance, which is a result of the thin ZIF-8 film layer. Meanwhile, the relatively low SF_6 permeance, i.e., few defects in the membranes also contributed to the high C_2H_4/C_2H_6 separation selectivity, in which the diffusion of the C_2H_4 molecules (kinetic diameter of 0.41 nm) through the microporous ZIF-8 structure are favored over those of C_2H_6 (kinetic diameter of 0.44 nm).

4. Conclusions

High quality and ultra-thin ZIF-8 membranes were evaluated for C_2H_4/C_2H_6 separation, with particular emphasis on the effects of temperature. Higher selectivity and permeability were observed at lower temperature. The adsorption of C_2H_6 is stronger than that of C_2H_4, which resulted in a lower C_2H_4/C_2H_6 mixture selectively compared to the ideal selectivity. However, due to the large surface barrier to the large molecule C_2H_6, the membrane is C_2H_4 selective under all studied conditions. The low thickness of the ZIF-8 membrane and clean support contributed to the high permeance while the selectivity was comparable to previously reported values because of the low density of defects in the ZIF-8 film layer as indicated by the low large molecules SF_6 permeance.

CRediT authorship contribution statement

Marta Pérez Miana: Investigation, Validation, Formal analysis, Writing – original draft. **Joaquín Coronas:** Supervision, Funding acquisition, Writing – review & editing. **Jonas Hedlund:** Conceptualization, Funding acquisition, Writing – review & editing. **Liang Yu:** Methodology, Supervision, Formal analysis, Funding acquisition, Writing – review & editing.

Table 2
Comparison of reported permeances and selectivities for the C_2H_4/C_2H_6 mixture using various membranes.

Type of membranes	Permeance (10^{-7} mol/(m^2·s·Pa))		Selectivity C_2H_4/C_2H_6	Operating conditions	Membrane thickness	Ref.
	C_2H_4	C_2H_6				
ZIF-8	8.2	3.3	2.5	−30 °C, 1 bar	600 nm	This work
ZIF-8	4.3	1.9	2.2	Room T, 1 bar	600 nm	This work
ZIF-8	0.8	0.4	2.0	Room T, 1 bar	~5 μm	James et al., 2017 [32]
ZIF-8	0.85	0.4	–	Room T 2 atm	~5 μm	James et al., 2020 [45]
ZIF-8	0.2	0.1	2.6	Room T, 1 bar	25 μm	Bux et al., 2011 [31]
ZIF-8	7.0	5.2	1.3	Room T, 1 bar	–	Valadez Sánchez et al., 2020 [46]
	1.6	0.8	2.1	Room T, 1 bar	–	
Polyimide	0.8	0.3	4.4	35 °C, 0.5 bar	25 μm	Staudt-Bickel et al., 2000 [11]
Co-Polyimides	8×10^{-5}	1.3×10^{-5}	6.8	35 °C, 2 atm	~50 μm	Chan et al., 2003 [9]
Zeolite AgX membrane	0.9	5.6×10^{-2}	16	30 °C, 1 atm	3.5 μm	Sakai et al., 2019 [24]

Declaration of Competing Interest

The authors declare the following financial interests/personal relationships which may be considered as potential competing interests:

J. Hedlund has founded the spin-off company ZeoMem Sweden AB with the goal to commercialize ultra-thin zeolite membranes for gas separations and he is the inventor of several patent applications in the area. The two most recent ones have the numbers US2016023187A1 and WO2019048505A1. He is also an inventor of a patent application with number WO2014140296A1 regarding the preparation of small MFI crystals.

L. Yu is an inventor of a patent application with number WO2019048505A1 describing the preparation of ultra-thin zeolite membranes. He is also a co-owner of ZeoMem Sweden AB.

The other authors have no competing interests to declare.

Data availability

Data will be made available on request.

Acknowledgements

Financial support from the grants PID2019-104009RB-I00 funded by MCIN/AEI/10.13039/501100011033 and T68_23R from the Aragón Government is gratefully acknowledged. M. P.-M. thanks also the Aragón Government for her PhD grant and Fundación CAI for her grant intended to cover the costs of the stay, as well as for a scholarship in the Iberus + project managed by Campus Iberus and co-financed by the Erasmus + program of the European Union. Bio4Energy, a Strategic Research Environment supported through the Swedish Government's Strategic Research Area initiative is also acknowledged for the financial support of this work.

References

[1] J. Hou, P. Liu, M. Jiang, L. Yu, L. Li, Z. Tang, Olefin/paraffin separation through membranes: from mechanisms to critical materials, J. Mater. Chem. A 7 (2019) 23489–23511, https://doi.org/10.1039/C9TA06329C.
[2] M.B. Leo, A. Dutta, S. Farooq, Process synthesis and optimization of heat pump assisted distillation for ethylene-ethane separation, Ind. Eng. Chem. Res. 57 (2018) 11747–11756, https://doi.org/10.1021/acs.iecr.8b02496.
[3] H. Strathmann, Membrane Separation Processes, 1. Principles, in: Ullmann's Encyclopedia of Industrial Chemistry, John Wiley & Sons, Ltd, 2011, doi: 10.1002/14356007.a16_187.pub3.
[4] R.W. Baker, Future directions of membrane gas separation technology, Ind. Eng. Chem. Res. 41 (2002) 1393–1411, https://doi.org/10.1021/ie0108088.
[5] A. Roy, S.R. Venna, G. Rogers, L. Tang, T.C. Fitzgibbons, J. Liu, H. McCurry, D. J. Vickery, D. Flick, B. Fish, Membranes for olefin–paraffin separation: an industrial perspective, Proc. Natl. Acad. Sci. 118 (2021), e2022194118, https://doi.org/10.1073/pnas.2022194118.
[6] W.J. Koros, C. Zhang, Materials for next-generation molecularly selective synthetic membranes, Nat. Mater. 16 (2017) 289–297, https://doi.org/10.1038/nmat4805.
[7] G.M. Iyer, L. Liu, C. Zhang, Hydrocarbon separations by glassy polymer membranes, J. Polym. Sci. 58 (2020) 2482–2517, https://doi.org/10.1002/pol.20200128.
[8] M. Rungta, C. Zhang, W.J. Koros, L. Xu, Membrane-based ethylene/ethane separation: the upper bound and beyond, AIChE J. 59 (2013) 3475–3489, https://doi.org/10.1002/aic.14105.
[9] S.S. Chan, T.-S. Chung, Y. Liu, R. Wang, Gas and hydrocarbon (C2 and C3) transport properties of co-polyimides synthesized from 6FDA and 1,5-NDA (naphthalene)/Durene diamines, J. Membr. Sci. 218 (2003) 235–245, https://doi.org/10.1016/S0376-7388(03)00180-7.
[10] K. Tanaka, A. Taguchi, J. Hao, H. Kita, K. Okamoto, Permeation and separation properties of polyimide membranes to olefins and paraffins, J. Membr. Sci. 121 (1996) 197–207, https://doi.org/10.1016/S0376-7388(96)00182-2.
[11] C. Staudt-Bickel, W.J. Koros, Olefin/paraffin gas separations with 6FDA-based polyimide membranes, J. Membr. Sci. 170 (2000) 205–214, https://doi.org/10.1016/S0376-7388(99)00351-8.
[12] P. Li, T.S. Chung, D.R. Paul, Gas sorption and permeation in PIM-1, J. Membr. Sci. 432 (2013) 50–57, https://doi.org/10.1016/j.memsci.2013.01.009.
[13] O. Salinas, X. Ma, E. Litwiller, I. Pinnau, Ethylene/ethane permeation, diffusion and gas sorption properties of carbon molecular sieve membranes derived from the prototype ladder polymer of intrinsic microporosity (PIM-1), J. Membr. Sci. 504 (2016) 133–140, https://doi.org/10.1016/j.memsci.2015.12.052.
[14] O. Salinas, X. Ma, E. Litwiller, I. Pinnau, High-performance carbon molecular sieve membranes for ethylene/ethane separation derived from an intrinsically microporous polyimide, J. Membr. Sci. 500 (2016) 115–123, https://doi.org/10.1016/j.memsci.2015.11.013.
[15] M. Rungta, G.B. Wenz, C. Zhang, L. Xu, W. Qiu, J.S. Adams, W.J. Koros, Carbon molecular sieve structure development and membrane performance relationships, Carbon 115 (2017) 237–248, https://doi.org/10.1016/j.carbon.2017.01.015.
[16] L. Xu, M. Rungta, W.J. Koros, MatrimidÂ® derived carbon molecular sieve hollow fiber membranes for ethylene/ethane separation | Elsevier Enhanced Reader, J. Membr. Sci. 380 (2011) 138–147, https://doi.org/10.1016/j.memsci.2011.06.037.
[17] J.E. Bachman, Z.P. Smith, T. Li, T. Xu, J.R. Long, Enhanced ethylene separation and plasticization resistance in polymer membranes incorporating metal–organic framework nanocrystals, Nat. Mater. 15 (2016) 845–849, https://doi.org/10.1038/nmat4621.
[18] P.J. Bereciartua, Á. Cantín, A. Corma, J.L. Jordá, M. Palomino, F. Rey, S. Valencia, E.W. Corcoran, P. Kortunov, P.I. Ravikovitch, A. Burton, C. Yoon, Y. Wang, C. Paur, J. Guzman, A.R. Bishop, G.L. Casty, Control of zeolite framework flexibility and pore topology for separation of ethane and ethylene, Science 358 (2017) 1068–1071, https://doi.org/10.1126/science.aao0092.
[19] G. Chen, X. Chen, Y. Pan, Y. Ji, G. Liu, W. Jin, M-gallate MOF/6FDA-polyimide mixed-matrix membranes for C2H4/C2H6 separation, J. Membr. Sci. 620 (2021), 118852, https://doi.org/10.1016/j.memsci.2020.118852.
[20] X. Chen, G. Chen, G. Liu, G. Liu, W. Jin, UTSA-280 metal–organic framework incorporated 6FDA-polyimide mixed-matrix membranes for ethylene/ethane separation, AIChE J. 68 (2022), e17688, https://doi.org/10.1002/aic.17688.
[21] A.F. Ismail, K.C. Khulbe, T. Matsuura, Gas separation membranes, Switz. Springer 10 (2015) 973–978.
[22] R.W. Baker, B.T. Low, Gas separation membrane materials: a perspective, Macromolecules 47 (2014) 6999–7013, https://doi.org/10.1021/ma501488s.
[23] V. Nikolakis, G. Xomeritakis, A. Abibi, M. Dickson, M. Tsapatsis, D.G. Vlachos, Growth of a faujasite-type zeolite membrane and its application in the separation of saturated/unsaturated hydrocarbon mixtures, J. Membr. Sci. 184 (2001) 209–219, https://doi.org/10.1016/S0376-7388(00)00623-2.
[24] M. Sakai, Y. Sasaki, T. Tomono, M. Seshimo, M. Matsukata, Olefin selective Ag-exchanged X-type zeolite membrane for propylene/propane and ethylene/ethane separation, ACS Appl. Mater. Interfaces 11 (2019) 4145–4151, https://doi.org/10.1021/acsami.8b20151.
[25] R. Wei, X. Liu, Z. Lai, MOF or COF membranes for olefin/paraffin separation: Current status and future research directions, Adv. Membr. 2 (2022), 100035, https://doi.org/10.1016/j.advmem.2022.100035.
[26] O.K. Farha, A. Özgür Yazaydın, I. Eryazici, C.D. Malliakas, B.G. Hauser, M.G. Kanatzidis, S.T. Nguyen, R.Q. Snurr, J.T. Hupp, De novo synthesis of a metal–organic framework material featuring ultrahigh surface area and gas storage capacities, Nat. Chem. 2 (2010) 944–948, doi: 10.1038/nchem.834.
[27] H. Li, M. Eddaoudi, M. O'Keeffe, O.M. Yaghi, Design and synthesis of an exceptionally stable and highly porous metal-organic framework, Nature 402 (1999) 276–279, https://doi.org/10.1038/46248.
[28] Z. Ji, H. Wang, S. Canossa, S. Wuttke, O.M. Yaghi, Pore chemistry of metal-organic frameworks, Adv. Funct. Mater. 30 (2020), 2000238, https://doi.org/10.1002/adfm.202000238.
[29] E.E. Sann, Y. Pan, Z. Gao, S. Zhan, F. Xia, Highly hydrophobic ZIF-8 particles and application for oil-water separation, Sep. Purif. Technol. 206 (2018) 186–191, https://doi.org/10.1016/j.seppur.2018.04.027.
[30] K.S. Park, Z. Ni, A.P. Côté, J.Y. Choi, R. Huang, F.J. Uribe-Romo, H.K. Chae, M. O'Keeffe, O.M. Yaghi, Exceptional chemical and thermal stability of zeolitic imidazolate frameworks, PNAS 103 (2006) 10186–10191, https://doi.org/10.1073/pnas.0602439103.
[31] H. Bux, C. Chmelik, R. Krishna, J. Caro, Ethene/ethane separation by the MOF membrane ZIF-8: molecular correlation of permeation, adsorption, diffusion, J. Membr. Sci. 369 (2011) 284–289, https://doi.org/10.1016/j.memsci.2010.12.001.
[32] J.B. James, J. Wang, L. Meng, Y.S. Lin, ZIF-8 membrane ethylene/ethane transport characteristics in single and binary gas mixtures, Ind. Eng. Chem. Res. 56 (2017) 7567–7575, https://doi.org/10.1021/acs.iecr.7b01536.
[33] Y. Sun, T. Ji, Y. Gao, J. Yan, Y. He, G. Xu, F. Yan, Q. Bian, Y. Liu, Freezing contra-diffusion: a new protocol for synthesizing Co-gallate MOF membranes toward superior ethylene/ethane separation performance, ACS Materials Lett. 5 (2023) 558–564, https://doi.org/10.1021/acsmaterialslett.2c01107.
[34] R. Wei, X. Liu, Z. Zhou, C. Chen, Y. Youyou, Z. Li, X. Li, X. Dong, D. Lu, Y. Han, Z. Lai, Carbon nanotube supported oriented metal organic framework membrane for effective ethylene/ethane separation, Sci. Adv. 8 (2022) eabm6741, doi: 10.1126/sciadv.abm6741.
[35] Y. Xiao, Y. Chu, S. Li, F. Chen, W. Gao, J. Xu, F. Deng, Host-guest interaction in ethylene and ethane separation on zeolitic imidazolate frameworks as revealed by solid-state NMR spectroscopy, Chem. – A Eur. J. 27 (2021) 11303–11308, doi: 10.1002/chem.202101779.
[36] C. Zhang, R.P. Lively, K. Zhang, J.R. Johnson, O. Karvan, W.J. Koros, Unexpected molecular sieving properties of zeolitic imidazolate framework-8, J. Phys. Chem. Lett. (n.d.), doi: 10.1021/jz300855a (accessed December 19, 2022).
[37] Y. Pan, Y. Liu, G. Zeng, L. Zhao, Z. Lai, Rapid synthesis of zeolitic imidazolate framework-8 (ZIF-8) nanocrystals in an aqueous system, Chem. Commun. 47 (2011) 2071–2073, https://doi.org/10.1039/c0cc05002d.
[38] J. Hedlund, J. Sterte, M. Anthonis, A.-J. Bons, B. Carstensen, N. Corcoran, D. Cox, H. Deckman, W. De Gijnst, P.-P. De Moor, F. Lai, J. McHenry, W. Mortier,

J. Reinoso, J. Peters, High-flux MFI membranes, Microporous Mesoporous Mater. 52 (2002) 179–189, https://doi.org/10.1016/S1387-1811(02)00316-5.
[39] J. Hwang, H. Azzan, R. Pini, C. Petit, H 2, N 2, CO 2, and CH 4 unary adsorption isotherm measurements at low and high pressures on zeolitic imidazolate framework ZIF-8, J. Chem. Eng. Data 67 (2022) 1674–1686, https://doi.org/10.1021/acs.jced.1c00900.
[40] L. Zhang, G. Wu, J. Jiang, Adsorption and diffusion of CO_2 and CH_4 in zeolitic imidazolate framework-8: effect of structural flexibility, J. Phys. Chem. C 118 (2014) 8788–8794, https://doi.org/10.1021/jp500796e.
[41] M. Masoudi-Nejad, S. Fatemi, Thermodynamic adsorption data of CH4, C2H6, C2H4 as the OCM process hydrocarbons on SAPO-34 molecular sieve, J. Ind. Eng. Chem. 20 (2014) 4045–4053, https://doi.org/10.1016/j.jiec.2013.12.107.
[42] J.-R. Li, R.J. Kuppler, H.-C. Zhou, Selective gas adsorption and separation in metal–organic frameworks, Chem. Soc. Rev. 38 (2009) 1477, https://doi.org/10.1039/b802426j.
[43] J. Hedlund, M.S. Nobandegani, L. Yu, The origin of the surface barrier in nanoporous materials, J. Membr. Sci. 641 (2022), 119893, https://doi.org/10.1016/j.memsci.2021.119893.
[44] G. Sastre, J. Kärger, D.M. Ruthven, Surface barriers and symmetry of adsorption and desorption processes, Adsorption 27 (2021) 777–785, https://doi.org/10.1007/s10450-020-00260-1.
[45] J.B. James, L. Lang, L. Meng, J.Y.S. Lin, Postsynthetic modification of ZIF-8 membranes via membrane surface ligand exchange for light hydrocarbon gas separation enhancement, ACS Appl. Mater. Interfaces 12 (2020) 3893–3902, https://doi.org/10.1021/acsami.9b19964.
[46] E.P. Valadez Sánchez, H. Gliemann, K. Haas-Santo, W. Ding, E. Hansjosten, J. Wohlgemuth, C. Wöll, R. Dittmeyer, α-Al2O3-supported ZIF-8 SURMOF membranes_diffusion mechanism of ethene/ethane mixtures and gas separation performance, Elsevier Enhanced Reader 594 (2020) 117421, doi: 10.1016/j.memsci.2019.117421.